PERSONALIZED COMPUTATION OF FRACTIONAL FLOW RESERVE IN CASE OF TWO CONSECUTIVE STENOSES

Yuri Vassilevski[1], Timur Gamilov[2] and Philip Kopylov[3]

[1]Institute of Numerical Mathematics RAS
Gubkina 8, Moscow, Russia, and
Moscow Institute of Physics and Technology
Instituskii Lane 9, Dolgoprudny, Russia
e-mail: yuri.vassilevski@gmail.com
[2] Moscow Institute of Physics and Technology
Instituskii Lane 9, Dolgoprudny, Russia, and
Institute of Numerical Mathematics RAS
Gubkina 8, Moscow, Russia e-mail: gamilov@crec.mipt.ru
[3] I.M. Sechenov First Moscow State Medical University
Trubetskaya ul., 8/2, Moscow, and
Institute of Numerical Mathematics RAS
Gubkina 8, Moscow, Russia

Keywords: Coronary vessels, Fractional Flow Reserve, Stenosis, Bifurcation, Wall-state equation

Abstract. *This paper addresses the problem of personalized computation of fractional flow reserve (FFR). FFR is considered to be the golden standard for making decision on surgical treatment of coronary vessels with multiple stenoses. Computer simulations could simplify the process by non-invasive estimation of FFR based on one-dimensional blood flow model. In this work a problem of two consecutive stenoses is studied. It is shown that in some cases only one of the stenoses has to be to removed, while the other one is insignificant. The structure of vessels is based on patient CT scans. An emphasis is made on the boundary conditions in bifurcation points of the vessels.*

1 Introduction

Heart diseases are the leading causes of sudden deaths in developed countries. One of the main reasons of heart failures are coronary stenoses. They can cause myocard ischemia which frequently results in disability or death. The main treatment of severe coronary stenosis is invasive endovascular intervention, i.e. stenting. Some stenoses can be treated with drugs without surgical intervention. Decision on the type of treatment is based on the estimate of haemodynamic importance of the lesion.

The modern golden standard for making decision on the type of treatment is the fractional flow reserve (FFR) [1, 2, 3]. FFR is defined as the ratio of average blood pressure distal to stenosis to average blood pressure in aorta under conditions of vasodilator administration [1]. Stenosis with FFR below 0.7-0.8 is considered to be severe and should be treated with endovascular surgical intervention. Stenosis with FFR above 0.8 can be treated with drug therapy. The FFR based assessment of stenosis helps to reduce the number of expensive operations as well as the number of incidences which caused disability or death [4].

Modern methods of the numerical FFR estimation involve 3D blood flow modelling in the local region of the studied vessel [1, 2]. It requires substantial computational resources but gives a detailed picture of blood flow. Another approach is based on 1D blood flow modelling of coronary region [5, 6]. One-dimensional approach allows to simulate substantial part of coronary region with several stenoses in different locations.

Cases with several stenoses complicate the FFR estimation [8, 9]. In some cases all lesions should be treated surgically while in others certain lesions can be ignored. 1D models allow to run a series of simulations for each surgical strategy and estimate its haemodynamical impact in a short time. In this work we demonstrate how 1D simulations can be used to study the interaction between two consecutive stenoses. The structure of computational domain was obtained from patient's CT-scans [10].

2 Methods

2.1 Blood flow model

The blood flow model used to estimate FFR considers unsteady viscous incompressible fluid flow through a 1D network of elastic tubes [6, 11]. The patient-specific network of coronary arteries was constructed on the basis of CT images [10]. In this section a brief description of the model is presented, for details we refer to [6, 11]. The flow in every vessel is described by mass and momentum balances

$$\partial A_k/\partial t + \partial (A_k u_k)/\partial x = 0, \tag{1}$$

$$\partial u_k/\partial t + \partial\left(u_k^2/2 + p_k/\rho\right)/\partial x = f_{fr}(A_k, u_k), \tag{2}$$

where k is the index of the vessel; t is the time; x is the distance along the vessel counted from the vessel junction point; ρ is the blood density (constant); $A_k(t, x)$ is the vessel cross-section area; p_k is the blood pressure; $u_k(t, x)$ is the linear velocity averaged over the cross-section; f_{tr} is the friction force. The relationship between pressure and cross-section is defined by the wall-state equation:

$$p_k(A_k) - p_{*k} = \rho_w c_k^2 f(A_k), \tag{3}$$

where ρ_w is the vessel wall density (constant); p_{*k} is the pressure in tissues surrounding the vessel; c_k defines elastic properties of the wall and can be considered as the speed of small

disturbances propagation [12]; $f(A_k)$ is defined by

$$f(A_k) = \begin{cases} \exp\left(A_k/A_{0k} - 1\right) - 1, & A_k/A_{0k} > 1 \\ \ln A_k/A_{0k}, & A_k/A_{0k} \leqslant 1, \end{cases} \tag{4}$$

A_{0k} is the unstressed vessel cross-sectional area.

At the entry point of the aorta the blood flow is assigned

$$u(t,0)\, A(t,0) = Q_H(t). \tag{5}$$

Here function $Q_H(t)$ corresponds to the heart rate value of 1 Hz and stroke volume of 65 ml [13].

At the bifurcation points the Poiseuille's pressure drop condition is used

$$p_k\left(A_k\left(t,\tilde{x}_k\right)\right) - p^l_{node}\left(t\right) = \varepsilon_k R^l_k\left(t,\tilde{x}_k\right) u_k\left(t,\tilde{x}_k\right), k = k_1, k_2, \ldots, k_M, \tag{6}$$

where R_k represents the hydraulic resistance of k-th vessel. Networks of veins and arteries are connected by similar pressure drop conditions.

At the terminal point of the venous system the pressure $p_H = 8mmHg$ is set as the boundary condition. The network of veins is considered to have the same structure as the network of arteries with doubled diameters and 20%-lowered c_k. To close the system, we add the mass conservation condition and second-order compatibility conditions of hyperbolic set (1),(2) (see [11]).

Myocardial compression during systolic phase is the essential part of coronary haemodynamics. The majority of perfusion occurs during the heart diastole [13]. Wall-state equation (3) is modified by setting $p_* = P^{cor}_{ext}(t)$. The shape of the function $P^{cor}_{ext}(t)$ is presented in [6] and it is similar to the pressure in the ventricle. The amplitude of P^{cor}_{ext} is 120 $mmHg$ and 30 $mmHg$ for terminal vessels of left and right coronary artery, respectively. Increased resistance of micro-circulation region during systole is simulated by multiplying R_k in (6) for all coronary vessels by the factor of 3 [14].

FFR is calculated as the ratio of average pressure in coronary artery distal to stenosis ($\overline{P}_{dist}$) to average aortic pressure ($\overline{P}_{aortic}$, aorta is vessel 1 in Fig. 1) during vasodilator administration:

$$FFR = \frac{\overline{P}_{dist}}{\overline{P}_{aortic}}. \tag{7}$$

Vasodilator administration is simulated by doubling S_0 in the studied vessel and decreasing resistance R by the factor of 5. This method provided good agreement with experimental results according to [6].

2.2 Compatibility conditions

Hyperbolic equations (1), (2) can be solved by different numerical methods. In this work we use the second-order grid-characteristic method [15]. The method requires the second-order approximation of compatibility conditions. A brief derivation of the second-order compatibility conditions is presented here. For more information we refer to [11].

Compatibility conditions of the hyperbolic set (1), (2) can be derived from characteristic form of (1) and (2):

$$\boldsymbol{\omega}_{ki} \cdot (\partial \mathbf{V}_k/\partial t + \partial \mathbf{F}_k/\partial x) = \boldsymbol{\omega}_{ki} \cdot (\partial \mathbf{V}_k/\partial t + \lambda_{ki}\partial \mathbf{V}_k/\partial x) = \boldsymbol{\omega}_{ki} \cdot \mathbf{g}_k, \quad i = 1, 2 \tag{8}$$

where λ_{ki} are the eigenvalues of the Jacobi matrix $\mathbf{A}_k = \partial \mathbf{F}_k/\partial \mathbf{V}_k$; $\boldsymbol{\omega}_{ki}$ are the eigenvectors of $\mathbf{A}_k$; $\mathbf{V}_k = (A_k, u_k)^T$; $\mathbf{F}_k = (A_k u_k, u^2_k/2 + p_k/\rho)^T$; $\mathbf{g}_k = (0, f_{fr})^T$.

After the finite differences discretization we can find linear dependence between the linear velocity $u_k(t_{n+1}, \tilde{x}_k)$ and the cross section area $A_k(t_{n+1}, \tilde{x}_k)$ at the time step t_{n+1} at the end or at the beginning of every vessel composing a junction node

$$u_k(t_{n+1}, \tilde{x}_k) = \alpha_k A_k(t_{n+1}, \tilde{x}_k) + \beta_k. \tag{9}$$

For each vessel we use an uniform 1D mesh composed of J edges:

$$M = \{(x_j, t_n) : x_j = hj, j = \overline{0, J}; t_n = \sum_{p=1}^{n} \tau_p\}$$

where h is the mesh size; τ_p is the p-th time step; L is the length of the vessel. For the beginning of the vessel outgoing from the junction node we use the second-order approximation of spatial derivative at time step t_{n+1}. Approximation of equation (8) ($i = 1$) is written at the point $(0, t_{n+1})$ as follows:

$$\left(\frac{\partial \mathbf{V}}{\partial x}\right)_{0,t_n} \approx \frac{-3\mathbf{V}_0^{n+1} + 4\mathbf{V}_1^{n+1} - \mathbf{V}_2^{n+1}}{2h},$$

$$\left(\frac{\partial \mathbf{V}}{\partial t}\right)_{0,t_n} \approx \frac{\mathbf{V}_0^{n+1} - \mathbf{V}_0^n}{\tau^{n+1}},$$

$$(\boldsymbol{\omega}_i)_{0,t_{n+1}} \approx (\boldsymbol{\omega}_i)_0^n, \quad (\lambda_i)_{0,t_{n+1}} \approx (\lambda_i)_0^n.$$

Denoting $w_0^n = \left(\sqrt{\frac{1}{\rho A}\left(\frac{\partial p}{\partial A}\right)}\right)_0^n$, $\mathbf{W}_0^n = \{w_0^n, (-1)^i\}$, $\sigma_0^n = \frac{\tau^{n+1}}{h}(\lambda_i)_0^n$ we obtain:

$$\mathbf{W}_0^n \cdot \left(\frac{(\mathbf{V}_0^{n+1}) - \mathbf{V}_0^n}{\tau^{n+1}} + (\lambda_i)_0^n \frac{-3\mathbf{V}_0^{n+1} + 4\mathbf{V}_1^{n+1} - \mathbf{V}_2^{n+1}}{2h}\right) = \mathbf{W}_0^n \cdot \mathbf{g}_0^{n+1}.$$

After substitution $\sigma_0^n = \frac{\tau^{n+1}}{h}(\lambda_i)_0^n$ and taking the dot-product

$$w_0^n[S_0^{n+1} - S_0^n + \sigma_0^n(-\frac{3}{2}S_0^{n+1} + 2S_1^{n+1} - \frac{1}{2}S_2^{n+1})]-$$

$$-[u_0^{n+1} - u_0^n + \sigma_0^n(-\frac{3}{2}u_0^{n+1} + 2u_1^{n+1} - \frac{1}{2}u_2^{n+1})] = \tau^{n+1}(w_0^n\phi_0^{n+1} - \psi_0^{n+1})$$

we find α and β from (9) at x_0

$$\alpha = w_0^n, \quad \beta = [w_0^n(\sigma_0^n(2S_1^{n+1} - \frac{1}{2}S_2^{n+1}) - S_0^n)-$$

$$- (\sigma_0^n(2u_1^{n+1} - \frac{1}{2}u_2^{n+1}) - u_0^n) - \tau^{n+1}(w_0^n\phi_0^{n+1} - \psi_0^{n+1})]/(1 - \frac{3}{2}\sigma_0^n). \tag{10}$$

In the similar way we derive α and β from (9) at x_J:

$$\alpha = -w_J^n, \quad \beta = [-w_J^n(\sigma_J^n(\frac{1}{2}S_{J-2}^{n+1} - 2S_{J-1}^{n+1}) - S_J^n)-$$

$$- (\sigma_J^n(\frac{1}{2}u_{J-2}^{n+1} - 2u_{J-1}^{n+1}) - u_J^n) + \tau^{n+1}(w_J^n\phi_J^{n+1} + \psi_J^{n+1})]/(1 + \frac{3}{2}\sigma_J^n). \tag{11}$$

Figure 1: The structure of reconstructed arterial part of anonymous patient-specific data set. Stars designate stenoses. Parameters of the vessels are presented in Tab. 1. LCA is the left main coronary artery, LAD is the left anterior descending artery, RCA is the right main coronary artery

k	l_k, cm	d_k, mm	$c_k, \frac{cm}{s}$	$R_k, \frac{ba \cdot s}{cm^3}$	k	l_k, cm	d_k, mm	$c_k, \frac{cm}{s}$	$R_k, \frac{ba \cdot s}{cm^3}$
1	5.28	21.7	1050	20	10	0.59	3.6	950	720
2	60.0	25.1	840	20	11	6.1	3.0	950	720
3	2.72	3.1	1200	7200	12	2.05	1.17	950	720
4	1.44	1.31	1200	7200	13	1.75	1.21	950	720
5	1.40	2.73	1200	7200	14	1.39	3.8	950	720
6	6.75	1.52	1200	7200	15	12.1	2.05	950	720
7	5.01	2.50	1200	7200	16	5.4	1.91	950	720
8	1.27	1.19	1200	7200	17	0.38	1.01	950	720
9	5.65	0.157	1200	7200	18	2.62	1.19	950	720

Table 1: Parameters of the arterial tree: k is the index of the vessel according to Figure 1, l_k is the length, d_k is the diameter, c_k is the stiffness (3), R_k is the resistance (6). Veins are considered to have the same structure with c_k lowered by 20 %, d_k doubled.

2.3   Patient specific 1D coronary network

The 1D vascular network was generated on the basis of patient-specific data. Geometry of coronary vessels was extracted from CT scans with the help of image processing and segmentation algorithms described in [7]. The network is presented in Fig. 1.

In this work two consecutive stenoses are evaluated. The stenosis in LCA is one third of the vessel's length, the stenosis in LAD is a half of the vessel's length. Note that the patient had other stenoses which were removed from the model in order to investigate the interaction of two consecutive stenoses. Each stenosis was modelled by separating the hosting vessel into three parts: the stenosed part, the proximal part and the distal part [6]. The parameters of the proximal and distal parts correspond to the parameters of the hosting non-stenosed vessel. The parameters of the stenosed part were modified: $A_{0_{stenosed}} = (1 - \gamma)^2 A_0$, $R_{stenosed} = \frac{L_{sten}}{L(1-\gamma)^4} R$, where γ is the stenosis fraction (degree of stenosis), R is the resistance of the hosting vessel, L is the length of the hosting vessel, L_{sten} is the length of the stenosed part of the vessel.

3   Results

Three series of simulations were performed for three degrees of stenosis in LCA: no stenosis 0%; slight stenosis 25%; severe stenosis 90%. In each series FFR in LAD was calculated, results are shown in Fig. 2. FFR in LCA was also calculated and turned to be independent of the degree of stenosis in LAD. In addition, we computed FFR in LCA for the following degrees of LCA stenosis: 0% gives FFR=0.96, 25% results in FFR=0.88, 90% results in FFR=0.5.
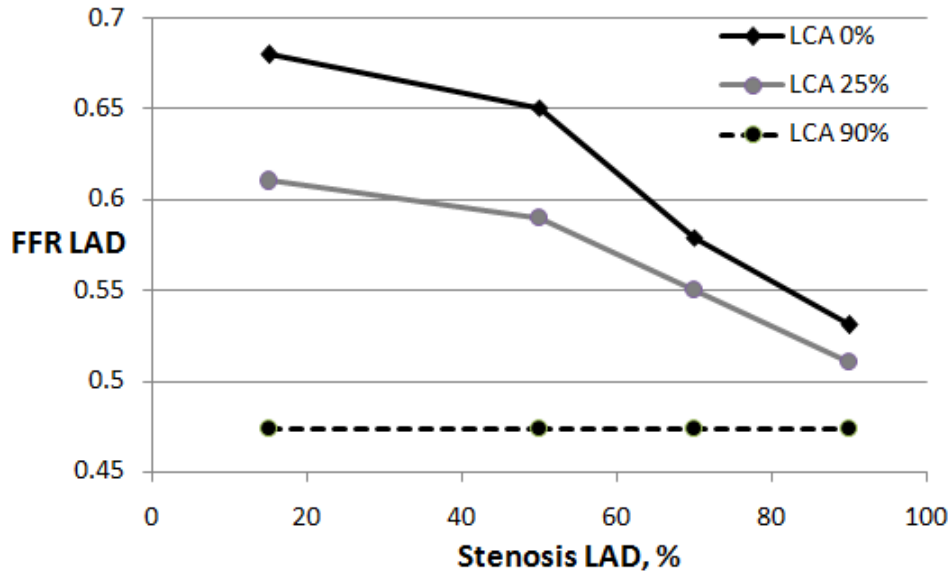

Figure 2: FFR in LAD for various stenosis degrees in LCA.

According to Fig. 2, FFR sensitivity to the degree of the distal stenosis depends on the degree of proximal stenosis. In the case of severe stenosis in LCA, the estimated FFR in LAD is independent of LAD degree of stenosis.

4   Conclusions

The results allow us to make a few conclusions. Firstly, longer lesions (LAD on Fig. 1) have significant impact on haemodynamics even when the degree of the stenosis is low. Secondly, the proximal stenosis has significant impact on FFR of the distal stenosis. The severe proximal stenosis nullifies blood flow to coronary arteries. As a result, lumen of distal arteries has little effect on haemodynamics: it can be very small and still be wide enough for a small amount of blood to flow through. This can be seen in Fig. 1 when the stenosis in LCA is 90%: FFR in LAD is constant since the distal stenosis does not affect the blood flow distribution. Therefore, FFR measurements for distal stenoses in presence of severe proximal lesion can be deceiving and do not allow to assess their impact on haemodynamics.

It should be noted that our method of virtual FFR estimation does not provide FFR=1.0 in case of 0% stenosis. The reason is boundary conditions (6) at the junction nodes that imply pressure drops in bifurcations. In order to achieve FFR=1.0 for healthy vessels, these conditions should be modified.

Cases with multiple stenoses are very hard to analyze without simulations. The presented method can be used for analysis of complicated cases with 3 or more lesions. The method

allows to study possible outcomes and choose the most cost efficient strategy of treatment of multiple stenoses.

REFERENCES

[1] P.D. Morris, D. Ryan,A.C. Morton, R. Lycett, P.V. Lawford, D.R. Hose, J.P. Gunn. Virtual fractional flow reserve from coronary angiography: Modeling the significance of coronary lesions. Results from the VIRTU-1 (VIRTUal fractional flow reserve from coronary angiography) study, *JACC: Cardiovascular Interventions*, **62**, 149–157, 2013.

[2] E.S. Bernad, S.I. Bernad, M.L. Craina. Hemodynamic parameters measurements to assess the severity of serial lesions in patient specific right coronary artery, *Bio-Medical Materials and Engineering*, **24(1)**, 323–334, 2014.

[3] Ph. Kopylov, A. Bykova, Yu. Vassilevski, S. Simakov. Role of measurement of fractional flow reserve (FFR) in coronary artery atherosclerosis, *Therapeutic archive*, **87(9)**, 106–113, 2015.

[4] C.K. Zarins, C.A. Taylor, J.K. Min. Computed fractional flow Reserve (FFTCT) derived from coronary CT angiography, *Journal of Cardiovascular Translational Research*, **6(5)**, 708–714, 2013.

[5] E. Boileau, P. Nithiarasu. One-dimensional modelling of the coronary circulation. Application to noninvasive quantification of fractional flow reserve (FFR), *Computational and Experimental Biomedical Sciences: Methods and Applications*, **21**, 137–155, 2015.

[6] T.M. Gamilov, P.Y. Kopylov, R.A. Pryamonosov, S.S. Simakov. Virtual fractional flow reserve assessment in patient-specific coronary networks by 1D hemodynamic model, *RJNAMM*, **30(5)**, 269–276, 2015.

[7] A.A. Danilov, Yu.A. Ivanov, R.A. Pryamonosov, Yu.V. Vassilevski. Methods of graph network reconstruction in personalized medicine. *Int.J.Numer.Meth.Biomed.Engng.*, e02754, 2016.

[8] S.E. Razavi, R. Zanbouri, O. Arjmandi-Tash. Simulation of blood flow coronary artery with consecutive stenosis and coronary-coronary bypass, *Bioimpacts*, **1(2)**, 99–104, 2011.

[9] N. Saito, H. Matsuo, Y. Kawase, S. Watanabe, B. Bao, E. Yamamoto, H. Watanabe, K. Nakatsuma, K. Ueno, T. Kimura. In vitro assessment of mathematically-derived fractional flow reserve in coronary lesions with more than two sequential stenoses, *Journal of Invasive Cardiology*, **25 (12)**, 642–649, 2013.

[10] Yu.V. Vassilevski, A.A. Danilov, T.M. Gamilov, Yu.A. Ivanov, R.A. Pryamonosov, S.S. Simakov. Patient-specific anatomical models in human physiology, *RJNAMM*, **30(3)**, 185–201, 2015.

[11] S.S. Simakov, T.M. Gamilov TM, Y.N. Soe. Computational study of blood flow in lower extremities under intense physical load. *RJNAMM*, **28(5)**, 485–504, 2013.

[12] I. B. Wilkinson, J. R. Cockcroft, D. J. Webb. Pulse wave analysis and arterial stiffness *J. Cardiovasc. Pharmacol.*, **32, Suppl.3**, S33–7, 1998.

[13] W.F. Ganong. *Review of Medical Physiology*, Stamford, CT, Appleton and Lange, 1999.

[14] M.A. Vis, P.H. Bovendeerd, P. Sipkema, N. Westerhof. Effect of ventricular contraction, pressure, and wall stretch on vessels at different locations in the wall, *Am J Physiol Heart Circ Physiol*, **272**, H2963–H2975, 1997.

[15] K.M. Magometov, A.S. Kholodov. *Grid Characteristic Numerical Methods*. Nauka, Moscow, 1988 (In Russian).

[16] O.C. Zienkiewicz, R.C. Taylor. *The finite element method, Vol. I, 4th Edition*. McGraw Hill, 1989.

[17] J.T. Oden, T. Belytschko, I. Babuska, T.J.R. Hughes. Research directions in computational mechanics. *Computer Methods in Applied Mechanics and Engineering*, **192**, 913–922, 2003.

[18] J.H. Argyris, M. Papadrakakis, L. Karapitta. Elastoplastic analysis of shells with the triangular element TRIC. M. Papadrakakis, A. Samartin, E. Oñate eds. *4th International Colloquium on Computation of Shell and Spatial Structures (IASS-IACM 2000)*, Chania, Crete, Greece, June 4-7, 2000.